Article

Cell Reports

Clonal Variation in Drug and Radiation Response among Glioma-Initiating Cells Is Linked to Proneural-Mesenchymal Transition

Graphical Abstract

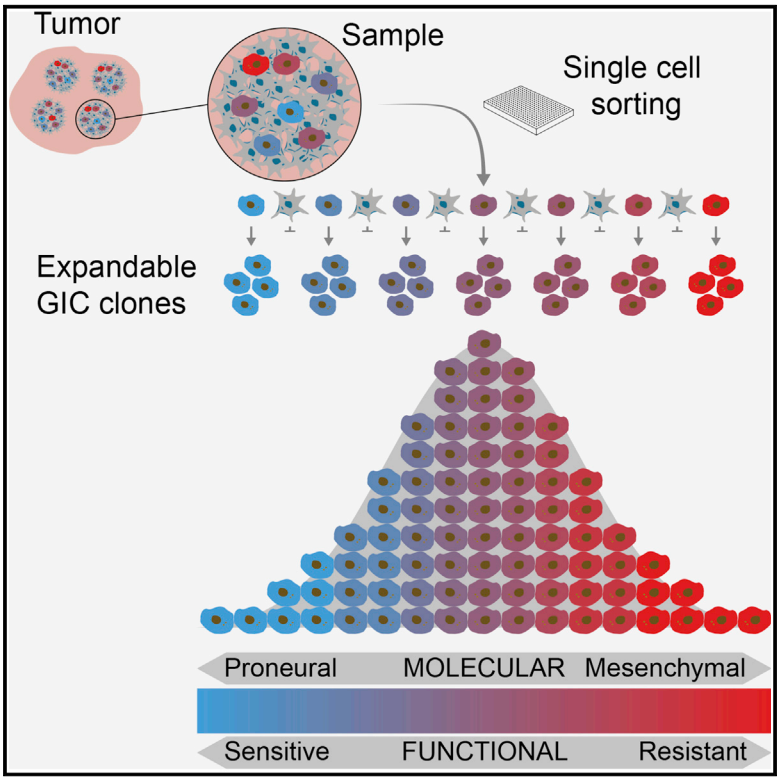

Authors

Anna Segerman, Mia Niklasson, Caroline Haglund, ..., Mårten Fryknäs, Bo Segerman, Bengt Westermark

Correspondence

anna.segerman@igp.uu.se (A.S.), bo.segerman@igp.uu.se (B.S.), bengt.westermark@igp.uu.se (B.W.)

In Brief

Heterogeneity in drug and radiation response among cancer-initiating cells complicates treatment and leads to relapse. Segerman et al. examine clonal variability among glioma-initiating cells and find a widespread and extensive heterogeneity in treatment response linked to a proneural-mesenchymal transition.

Highlights

- Intratumoral heterogeneity of glioblastoma is captured by clone libraries
- Pre-existing multitherapy-resistant glioma cells have a mesenchymal character
- A gradient of therapy resistance is linked to a proneural-mesenchymal axis
- Therapy resistance is associated with an altered DNA methylation pattern

Accession Numbers

GSE89401
GSE89398
GSE89399
GSE89400

Segerman et al., 2016, Cell Reports *17*, 2994–3009
December 13, 2016
http://dx.doi.org/10.1016/j.celrep.2016.11.056

OPEN ACCESS
CellPress

Cell Reports
Article

Clonal Variation in Drug and Radiation Response among Glioma-Initiating Cells Is Linked to Proneural-Mesenchymal Transition

Anna Segerman,[1,3,*] Mia Niklasson,[1] Caroline Haglund,[2] Tobias Bergström,[1] Malin Jarvius,[2] Yuan Xie,[1] Ann Westermark,[1] Demet Sönmez,[1,6] Annika Hermansson,[1] Marianne Kastemar,[1] Zeinab Naimaie-Ali,[1] Frida Nyberg,[2] Malin Berglund,[2] Magnus Sundström,[1] Göran Hesselager,[4] Lene Uhrbom,[1] Mats Gustafsson,[2] Rolf Larsson,[2] Mårten Fryknäs,[2] Bo Segerman,[1,5,*] and Bengt Westermark[1,7,*]

[1]Department of Immunology, Genetics and Pathology, Science for Life Laboratory, Rudbeck Laboratory, Uppsala University, 751 85 Uppsala, Sweden
[2]Department of Medical Sciences, Cancer Pharmacology and Computational Medicine, Uppsala University, Uppsala University Hospital, 751 85 Uppsala, Sweden
[3]Clinical Chemistry and Pharmacology, Uppsala University Hospital, 751 85 Uppsala, Sweden
[4]Department of Neurosurgery, Uppsala University Hospital, 751 85 Uppsala, Sweden
[5]National Veterinary Institute, 750 07 Uppsala, Sweden
[6]Present address: Pfizer, Vetenskapsvägen 10, 191 90 Sollentuna, Sweden
[7]Lead Contact
*Correspondence: anna.segerman@igp.uu.se (A.S.), bo.segerman@igp.uu.se (B.S.), bengt.westermark@igp.uu.se (B.W.)
http://dx.doi.org/10.1016/j.celrep.2016.11.056

SUMMARY

Intratumoral heterogeneity is a hallmark of glioblastoma multiforme and thought to negatively affect treatment efficacy. Here, we establish libraries of glioma-initiating cell (GIC) clones from patient samples and find extensive molecular and phenotypic variability among clones, including a range of responses to radiation and drugs. This widespread variability was observed as a continuum of multitherapy resistance phenotypes linked to a proneural-mesenchymal shift in the transcriptome. Multitherapy resistance was associated with a semi-stable cell state that was characterized by an altered DNA methylation pattern at promoter regions of mesenchymal master regulators and enhancers. The gradient of cell states within the GIC compartment constitutes a distinct form of heterogeneity. Our findings may open an avenue toward the development of new therapeutic rationales designed to reverse resistant cell states.

INTRODUCTION

The stem cell model of cancer is based on the concept that the progressive growth of a tumor is fueled by a subpopulation of cells with stem cell-like characteristics, called cancer stem cells (CSCs) (Bonnet and Dick, 1997; Visvader and Lindeman, 2008). The CSC model is not contradictory to the widely accepted clonal evolution model of cancer, according to which accumulation of mutations (and/or epigenetic changes) and selection of cells with increased fitness in the tumor microenvironment leads to clonal expansions. Experimentally, CSCs are defined as cancer cells that can self-renew, generate a differentiated progeny, and most importantly, initiate new tumors. The operational term tumor-initiating cell (TIC) is wider and can be used to describe all cancer cells with tumorigenic potential (Lathia et al., 2015). Genetic or epigenetic heterogeneity within the TIC compartment may be the basis for outgrowth of pre-existing resistant subpopulations in conjunction with treatment failure. Given the role of TICs as the drivers of tumor growth, they constitute an obvious therapeutic target.

The extremely poor prognosis of glioblastoma multiforme (GBM) is a strong incentive for studying TIC biology in this particular tumor. It is one of the most aggressive human cancers, with a median survival of 15 months, and is in nearly all cases fatal. The exceptionally invasive growth of GBM precludes radical surgery, and despite aggressive treatment with radiotherapy and concomitant adjuvant chemotherapy with temozolomide (TMZ), the tumor inevitably relapses (Stupp et al., 2005). Four molecular subtypes of GBM have been described, proneural (PN), classical (CL), neural (N), and mesenchymal (MES) (Verhaak et al., 2010), based on the genetic and RNA expression profiles of GBM samples. Different subtypes can co-exist in the same tumor, both at the regional (Sottoriva et al., 2013) and at the single-cell level (Patel et al., 2014), and shift in subtype occurs in patients and can be induced in experimental systems (Bhat et al., 2013; Halliday et al., 2014; Phillips et al., 2006).

Experimental studies of the functional consequences of the molecular heterogeneity in the TIC compartment are highly warranted but essentially lacking, particularly in solid tumors. Such studies have been hampered by difficulties in establishing single-cell-derived cultures from tumor explants. A step forward was taken by Meyer et al. (2015), who established clonal cultures from fresh GBM tissue, allowing functional studies on the glioma-initiating cell (GIC) population. When cultured in defined neural stem cell medium (Pollard et al., 2009; Singh et al., 2003), the GICs retain the phenotypic and molecular profile of

A

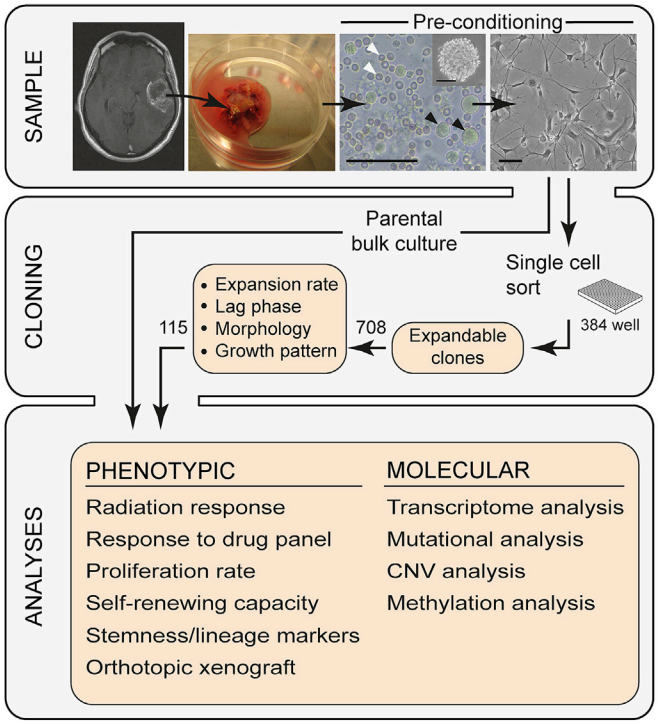

B

Patient	A	B	B	C	D	E
Bulk culture	U3065MG	U3117MG	U3118MG	U3167MG	U3017MG	U3121MG
Diagnosis	GB, IV	GB, IV	GB, IV	GB, IV	GB, IV	GB, IV
Age at diagnosis	77	57	57	58	68	64
Survival (days)	94	310	310	1234	442	479
Sex	M	M	M	F	M	M
Expandable clones	51	124	303	111	112	7
Chr10 loss/LOH	✓	✓	✓	✓	✓	✓
Chr7 gain	✓	✓	✓	✓	✓	✓
EGFR f.a.	-	-	-	-	-	✓
MDM4 f.a.	✓	-	-	-	-	✓
MDM2 f.a.	-	-	-	✓	-	-
CDK4 f.g.	-	-	-	-	-	✓
CDKN2A/B h.d.	✓	✓	✓	✓	✓	✓
PTEN mut.	✓	-	-	-	-	-
RB1 mut.	-	-	-	-	✓	-
EFGRvIII mut.	-	-	-	-	-	✓
IDH1 mut.	-	-	-	-	-	-
NF1 mut.	-	-	-	-	-	-
PI3K mut.	-	-	-	-	-	-
P53 mut.	-	-	-	-	-	-
MET mut.	-	-	-	-	-	-
PDGFRA mut.	-	-	-	-	-	-
MGMT promoter methylated	✓	-	-	✓	-	-

C

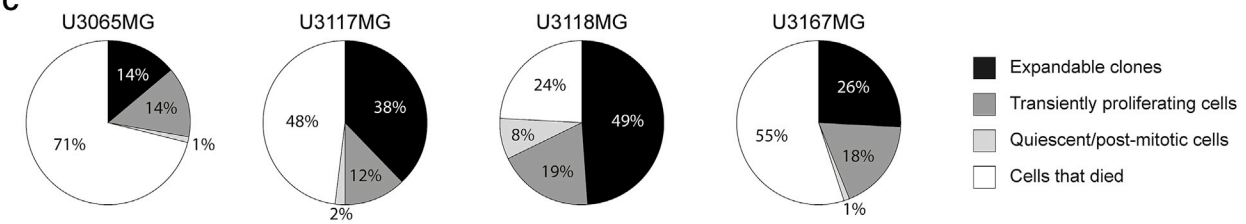

D

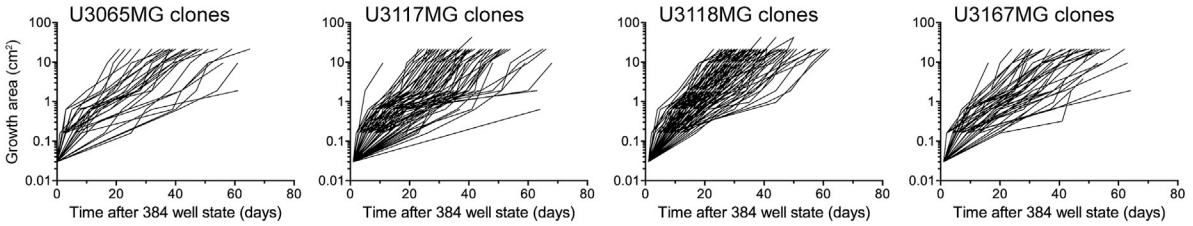

E

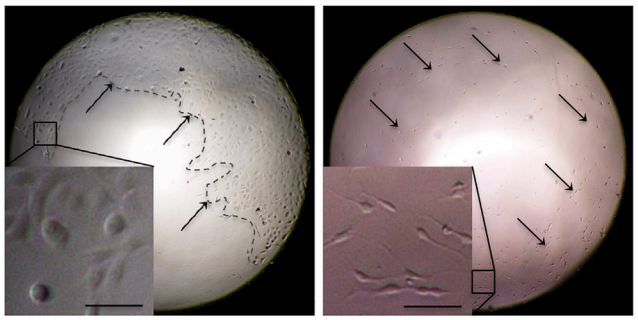

F

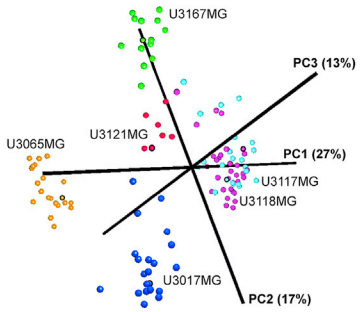

(legend on next page)

the primary tumor (Lee et al., 2006; Xie et al., 2015). However, knowledge on how molecular heterogeneity within the GIC compartment is translated into functional properties is still fragmentary and is the focus of the current study.

Here we show that a single GBM gives rise to a spectrum of GIC clones with varying degrees of drug resistance and radioresistance and that GIC clones displaying resistance to one type of therapy also are resistant to several other therapies. The variation in multitherapy resistance is tightly linked to a molecular signature along a continuous PN-MES subtype axis. The heterogeneity along the PN-MES axis was associated with altered DNA methylation of MES transition master regulators and thus appears to be generated by slow epigenetic drift. Altogether, this work adds valuable knowledge of the intratumoral GIC heterogeneity and may be exploited in future attempts to reprogram GICs to render them sensitive to therapy.

RESULTS

Clonal Glioma-Initiating Cell Cultures Capture Intratumoral Heterogeneity

To create a platform for functional studies of intratumoral heterogeneity in the GIC population, we established libraries of single-cell-derived cultures from fresh surgical specimens from five patients with treatment-naive GBM. An adherent neural stem cell culturing protocol was used to enrich for cells with stem-like properties and to permit efficient phenotypic screening (Pollard et al., 2009).

Six clone libraries with a total of 708 clones were produced, two of which originated from separate surgical samples of the same tumor (Figures 1A and 1B). In parallel, the parental cultures were expanded as references. All parental cultures displayed the typical GBM alterations: gain in chromosome (chr) 7, loss or loss of heterozygosity (LOH) in chr10, and homozygous deletion of *CDKN2A/B* (Figures 1B and S1A). There were also patient-specific alterations, which included *EGFR*, *MDM2*, *MDM4*, *CDK4*, *PTEN*, and *RB1* (Figures 1B and S1A; Table S1). The two samples originating from the same patient differed only in the signal strength of copy number variations (CNVs) in chr12, chr19, and chr22 (Figure S1A).

The cloning results suggested that the original primary cultures were heterogeneous in terms of the cells' self-renewal capacity with four discernible categories: (1) expandable clones, (2) transiently proliferating cells, (3) quiescent or post-mitotic cells, and (4) single cells that died during the culture period (Figure 1C). The current study is focused on the clonogenic GIC fraction.

The GIC clones varied in terms of initial expansion rate (Figure 1D) and lag phase, but there was no link between these properties (Figure S1B). Moreover, clones were heterogeneous in morphology and growth pattern (Figure 1E).

We selected 115 clones, representative for the variation in initial growth characteristics and morphology, for further phenotypic and molecular characterization. Principal-component analysis (PCA) of the transcriptomes revealed a high degree of variability within the libraries (Figure 1F), although "patient-to-patient" variation was larger. The two libraries derived from the same patient were similar.

In summary, the clone libraries capture both phenotypic and molecular heterogeneity within the GIC compartment. They allow for linked functional and molecular profiling and thus constitute a valuable model system to decipher GIC heterogeneity.

A Continuous Multidrug and Radiotherapy Resistance Phenotype Gradient Exists in Each GIC Clone Library

To study the impact of clonal GIC heterogeneity with regard to treatment response, each of the 115 selected clones and the parental cultures were exposed to γ-radiation and a panel of 15 chemical agents, including clinically relevant drugs (such as TMZ) and representing different mechanisms of action. The drugs target known vulnerabilities of cancer cells, as well as key signaling pathways in GBM (Figure 2A).

All GIC clone libraries displayed extensive clonal variability in radiation sensitivity phenotypes, with limited additive effects of TMZ (Figures 2B and 2C; Table S2). The U3065MG clones exhibited the most heterogeneous response, with variability comparable to that seen among different parental cultures (Figure 2C). There were also large clonal variations in responses to the drug panel, especially in the U3065MG and U3017MG libraries (Figure 2D; Table S2). In all libraries, a substantial fraction of the clones was far more drug- and radioresistant than their corresponding parental culture, which typically showed low to intermediate resistance relative to its library (Figures 2C–2E; Table S2).

Figure 1. Clonal GIC Cultures from Primary Glioblastomas Capture Intratumoral Heterogeneity

(A) Workflow for the establishment, molecular profiling, and phenotypic characterization of clone libraries established from primary GBM patient sample cultures. The GBM surgical sample was dissociated into a cell suspension containing tumor cells (black arrowheads), debris, and blood cells (white arrowheads). After tumor sphere formation (insert), the spheres were dissociated and briefly cultured on laminin-coated dishes before single-cell sorting and subsequent expansion of individual clones. Phenotypic and molecular analyses were performed. CNV, copy number variation. Scale bars, 50 μm.

(B) Patient information, number of expandable GIC clones in each library, and genetic profile (exon sequencing and CNV analysis; see Figure S1A and Table S1) of the parental cultures. LOH, loss of heterozygosity; fa, focal amplification; fg, focal gain; hd, homozygous deletion; mut, mutation. MGMT-methylated samples had >25% mean methylation. *2 years and 10 months post-diagnosis.

(C) The proportions of single-seeded cells from four patient samples that gave rise to expandable GIC clones, transiently proliferating cells, quiescent or post-mitotic cells, and cells that died during the culture period of 6 weeks.

(D) Variation in initial expansion rate (growth area followed between a confluent 384-plate well and a confluent 35-mm dish). Each line represents an individual clone.

(E) Variation in morphology and growth patterns within the U3117MG clone library at the initial 384-well plate state. Left: expansion as a continuous monolayer (arrows, monolayer border). Right: expansion dispersed over the surface of the well (arrows, single-spread cells). Scale bar, 50 μm.

(F) Variation in the transcriptome profile of 115 clones representing all libraries. Principal-component analysis (PCA) was based on the 5,000 most variable genes. See also Figure S1 and Table S1.

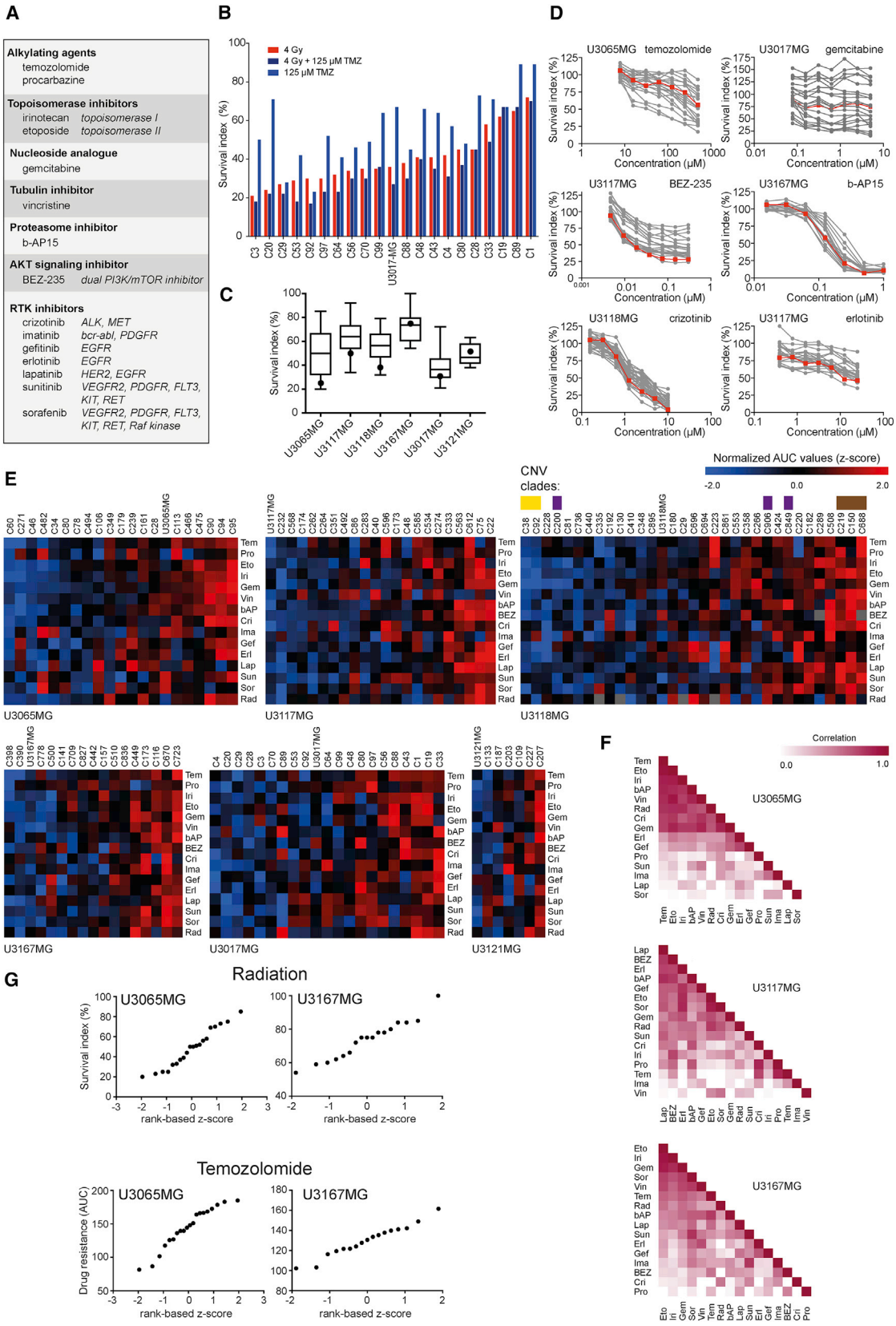

(legend on next page)

A striking observation was that clones resistant to one drug also tended to be resistant to most of the drugs in the panel, regardless of their mechanism of action (Figures 2E, 2F, and S2A). Moreover, radioresistance correlated with drug resistance, as shown in heatmaps of response values (Figure 2E) and similarity matrices (Figures 2F and S2A). Thus, these data define a multidrug and radiotherapy resistance phenotype, hereafter referred to as multitherapy resistance, within each library.

Resistance to specific receptor tyrosine kinase (RTK) inhibitors is negatively correlated with the expression of its target, and resistance to TMZ is known to correlate positively with the DNA repair enzyme MGMT (Hegi et al., 2005; Nathanson et al., 2014; Szerlip et al., 2012). We analyzed our data for such specific correlations, but only one was significant after correction for multiple testing (anaplastic lymphoma receptor tyrosine kinase [ALK] and crizotinib in U3118MG, $r = -0.68$, $p < 0.0001$) (Figure S2B), suggesting that a more general resistance mechanism dominated.

Another important observation was that the clones within a library did not fall into distinct response groups; rather, the differences in cell survival were best described as continuums of phenotypes (Figures 2B, 2D, and 2E; Table S2) that resembled normal distributions (Figure 2G). This indicates that the clonal variation in multitherapy resistance is a result of a dynamic process in the GIC population. Biological replicates showed that there was a high reproducibility in treatment response (Figure S2C). However, a few clones did change in their character, such as U3117MG-C232, which moved from a sensitive to an intermediate phenotype, and U3065MG-C113, which moved from a resistant to an intermediate phenotype (Figure S2C). Thus, the clones' phenotypes showed rigidity, but their continuous distribution, together with occasional examples of phenotypic drift, implies there was semi-stability.

Altogether, we found extensive variation in responses to drugs and radiation among GIC clones. There was a continuous gradient of multitherapy resistance phenotypes that dictated the responses of individual clones. The GIC phenotypes were largely stable, but our findings suggest that the variability has been formed by a slow fluctuation between semi-stable cell states. We next set out to understand the characteristics of these cell states.

Both Sensitive and Resistant Clones Exhibit Stem Cell Features and Form Xenograft Tumors Resembling High-Grade Gliomas

Multidrug and radiotherapy resistance is associated with stem cell traits (Bao et al., 2006; Bhat et al., 2013; Bleau et al., 2009; Liu et al., 2006); thus, we next examined the stem cell-associated features in the GIC clones. To estimate the self-renewal capacity, we reseeded the clones from four libraries as single cells and determined their secondary clone-forming ability. Cells that had undergone at least eight doublings after 4 weeks were considered clonogenic. Only one library displayed a negative correlation ($r = -0.46$, $p = 0.01$) between secondary clone formation and drug resistance (Figure 3A). The parental cultures were in all cases more clonogenic than most clonal derivatives (Figure 3A). A consistent link between secondary clone formation and multitherapy resistance was thus absent.

We next examined the expression of a set of stem cell markers. Immunofluorescence staining of selected sensitive and resistant clones showed that all cells were SOX2 positive and most cells were nestin positive, regardless of their drug- and radiation-response profile (Figures 3B, S3A, and S3B). The neural stem cell and GIC marker *PROMININ-1*/CD133 was inconsistently linked to resistance (Figures S3C and S3D). Hence, resistance was not associated with a general increase in expression of stem cell markers.

To confirm the tumor-forming ability of the cells, we injected 34 selected clones and the parental cultures from four libraries intracerebrally into neonatal non-obese diabetic-severe combined immunodeficiency (NOD-SCID) mice (Table S3). The mice were euthanized when disease symptoms appeared. All clones and parental cultures generated lesions with high-grade glioma features (Figures 3C–3J; Table S3), such as infiltrative growth (Figures 3C–3F, 3I, and 3J) and high mitotic activity (Figure 3H). The proportion of proliferating cells (Ki67 positive) within the tumors was usually >15% (Table S3). Pseudopalisading necrosis was absent, but apoptotic figures were frequent (Figure 3H). Both the penetrance and the propensity to form massive bulk tumors (examples shown in Figures 3C and 3D) varied among clones (Figure 3K; Table S3). However, we only found a clear link to the resistance phenotype in the U3065MG library, wherein all sensitive clones injected displayed a combination of diffuse growth and massive bulk tumor formation, whereas the resistant clones more frequently were restricted to diffuse growth (Figures 3C–3F). Moreover, resistant clones generated lesions on average >10 weeks later than sensitive clones (Figure 3K; Table S3).

In conclusion, multitherapy resistance seemed to be coupled to a change in GIC phenotype, distinct from an increase in stem cell-associated features and malignant potential.

Figure 2. A Continuous Multidrug- and Radiotherapy-Resistance Phenotype Gradient Exists in Each GIC Clone Library

(A) Drugs and targeted agents used in the treatment response assays. RTK, receptor tyrosine kinase.

(B) Response to 4 Gy γ-radiation ± TMZ (125 μM) in the U3017MG clone library 6 days after exposure to a single dose. See Table S2 for data on the other clone libraries.

(C) Variation in γ-radiation (4 Gy) response within the six clone libraries. The parental culture is indicated as a black dot.

(D) Selection of dose-response curves. Parental cultures are shown in red. See Table S2 for complete drug set data for all clone libraries and Figure S2C for a comparison between replicate experiments.

(E) Heatmap of drug and radiation response values (*Z* scores) for individual clones. Drug responses were quantified as area under the curve (AUC). Gray, not analyzed. Genetic clades, as defined in Figure 6B, are indicated in U3118MG (yellow, purple, and brown boxes).

(F) Similarity matrix (Pearson correlation) for drug (AUC *Z* score values) and radiation response profiles for three clone libraries. See Figure S2A for data on the other libraries.

(G) Quantile-quantile plot comparing the distribution of selected phenotypic data with a normal distribution.

See also Table S2.

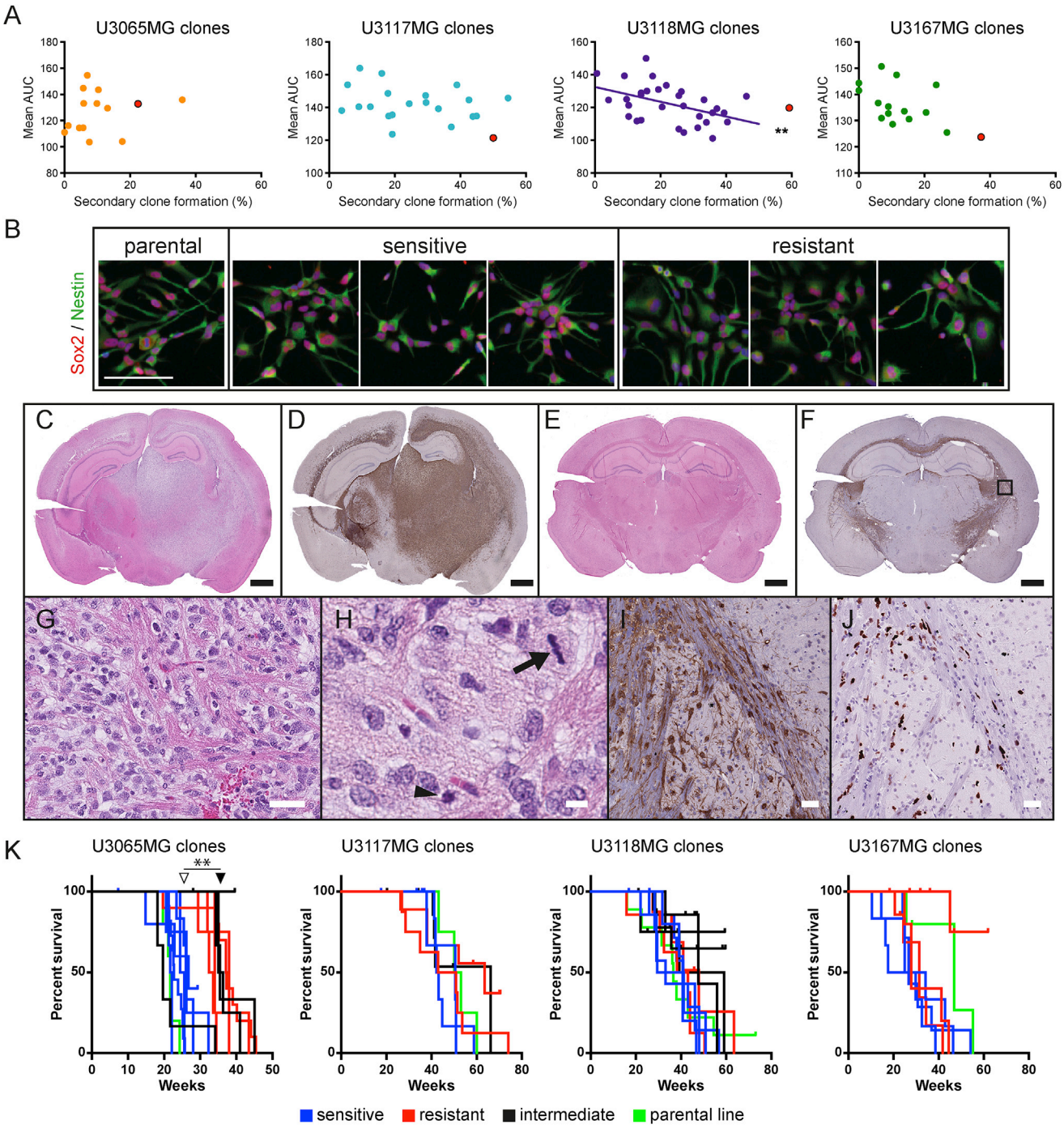

Figure 3. Both Sensitive and Resistant Clones Exploit Stem Cell Features and Form Xenograft Tumors Resembling High-Grade Gliomas

(A) Scatterplot between average drug response (mean AUC) and secondary clone formation for clones and parental cultures (red). Clonogenicity was measured by single-cell seeding in coated 384-well plates and counting cells that had undergone at least eight doublings ($\geq$256 cells) after 4 weeks. **$p < 0.01$ (Pearson).

(B) Immunostaining of Sox2 (red) and nestin (green) in three sensitive and three resistant clones, and the parental culture from the U3017MG library. Scale bar, 100 μm. See Figures S3A and S3B for staining of clones from four other libraries.

(C and D) Infiltrative macroscopically visible bulk tumor derived from a U3065MG clone intracerebral injection into NOD-SCID mice. (C) H&E staining and (D) human-specific antigen STEM121 immunostaining of coronal brain sections. Scale bar, 1 mm.

(E and F) Infiltrative diffuse growth after a U3065MG clone intracerebral injection into NOD-SCID mice. (E) H&E staining and (F) STEM121 immunostaining. Scale bar, 1 mm.

(legend continued on next page)

The Multitherapy-Resistant Phenotype Is Associated with a Mesenchymal Profile

To identify cellular processes and genes related to the multitherapy resistance, we analyzed the transcriptome data. Expression data were compared to phenotypic resistance scores based on the average of normalized response values to all drugs and radiation (see Experimental Procedures). Gene set enrichment analysis (GSEA) showed that multitherapy resistance was, with some library-specific differences, linked to processes such as mesenchymal transition (Anastassiou et al., 2011), extracellular matrix (ECM) receptor interactions, antigen processing and presentation, ATP-binding cassette (ABC) transporters, and drug metabolism (Figure 4A; Table S4). By contrast, sensitivity was associated with cell cycling and proliferation-related processes (Figure 4A; Table S4).

To identify specific genes associated with resistance or sensitivity, we selected genes with the largest positive and negative correlations to the phenotypic resistance score in each library (Table S5). The 5,000 genes with largest clonal variability were used, and the cutoffs were based on analysis with randomly shuffled phenotype data. The resistance- and sensitivity-associated genes included MES and PN subtyping genes, respectively (Table S5). Using a larger set of MES and PN subtyping genes (Verhaak et al., 2010) in gene similarity matrices (Pearson correlation), we found clear links between MES and resistance-associated genes and between PN and sensitivity-associated genes in all libraries (Figure 4B). There were also clear negative correlations between resistance- and sensitivity-associated genes (Figure 4B). Hence, in all clone libraries, there was an axis between two mutually exclusive cell states, with MES and resistance characteristics at one end and PN and sensitivity at the other end.

The GSEA indicated that sensitive clones were more proliferative, which also is an attribute of PN-like GBM cell lines (Beier et al., 2007; Ligon et al., 2007; Xie et al., 2015). In proliferation measurements, we found a correlation ($r = 0.84$, $p = 0.025$) between doubling time and phenotypic resistance score in the U3118MG library and similar trends in the other libraries (Figure 4C). In the U3117MG library, we observed a link ($r = 0.69$, $p = 0.0005$) between resistance and slower initial expansion rate during cloning (Figure S4A). Altogether, resistance was associated with slightly slower proliferative activity.

Although resistance was connected to MES genes and sensitivity was connected to PN genes in all clone libraries, there were variations in which specific subtype markers showed the strongest correlation. The commonly used PN GIC marker OLIG2 was negatively linked ($r = -0.48$, $p = 0.036$) and the MES GIC marker CD44 was positively linked ($r = 0.57$, $p = 0.010$) to the phenotypic resistance score in the U3017MG library (Figure 4D). Similar trends were seen for Olig2 in other libraries (Figure S4B). We also analyzed protein expression levels for Olig2 and CD44, as well as the mesenchymal stem cell and MES-associated fibronectin receptor integrin β1 in a selection of sensitive and resistant GIC clones. Olig2 protein levels were higher in U3065MG-sensitive clones than in resistant ones (Figures 4E and 4F); this was less clear in other libraries (Figures S4C and S4D). Nearly 100% of the cells expressed both CD44 and integrin β1, but resistant clones typically expressed higher levels of these markers than sensitive clones (Figures 4G and S4E).

In summary, the resistant cell state of GICs was associated with a MES character and sensitivity was associated with a PN character. Several concurrent resistance mechanisms were implicated by the GSEA results, including increased drug metabolism and transport, as well as slower cell cycling. Because there was a connection with GBM subtyping genes, we next aimed to relate our data to previously published GBM datasets.

A Gene Expression Signature for the Multitherapy-Resistant GIC State Identifies Gradients in Both Single-Cell and Tumor Sample Datasets

To obtain a robust gene expression signature for the resistance phenotype applicable on external datasets, all library-specific resistance-associated genes were combined and the 50 genes with largest average correlation coefficients across all libraries were selected (Figure 5A). Gene ontology analysis of this resistance signature highlighted primarily cell adhesion and ECM-related processes (Figure 5B). The mean expression of the signature genes was used as resistance signature metascores. These correlated with the phenotypic resistance scores in all libraries (Figures 5C and 5D), indicating good performance across patient samples.

Using a selected gene from the resistance signature, *CLMP*, we explored the possibility of predicting resistance in nine previously uncharacterized U3065MG clones. *CLMP* was the most variable among the ten highest-ranked resistance signature genes in this library. The qPCR data for *CLMP* correlated with the phenotypic resistance scores (Figure 5E), illustrating the potential role for resistance signature genes as predictive markers.

To test the stability of the molecular profiles, we compared resistance signature metascores of clones between replicate experiments. Similar to the result seen for the resistance phenotype (Figure S2C), the clones largely retained their molecular signature characteristics in independent experiments (Figures S5A and S5B). For the U3117MG-C232 clone that made a shift in resistance level between experiments, the signature metascore shifted in accordance with the phenotype (Figures S5A and S5B).

Next, we exploited our resistance signature in published GBM datasets. Our signature separated expression data from both single cells (Patel et al., 2014) and the Cancer Genome Atlas (TCGA) tumor samples (http://tcga-data.nci.nih.gov) into continuous

(G and H) H&E staining demonstrating high-grade glioma characteristics such as hypercellularity, cellular pleomorphism, and nuclear atypia (G), and mitosis (black arrow) and apoptotic figure (arrowhead) (H). Scale bars, 50 μm (G) and 10 μm (H).
(I) High magnification of box in (F) showing STEM121 staining. Scale bar, 50 μm.
(J) Proliferating cells (Ki67 staining) in a tumor with diffuse growth in the section adjacent to (I). Scale bar, 50 μm. See Table S3 for quantification of Ki67 staining.
(K) Kaplan-Meier survival curves of NOD-SCID mice injected with selected U3065MG, U3117MG, U3118MG, and U3167MG clones. Arrowheads in U3065MG indicate the median survival for sensitive clones (25.5 weeks) and resistant clones (35.6 weeks). **$p < 0.01$ (Mann-Whitney).
See also Figure S3 and Table S3.

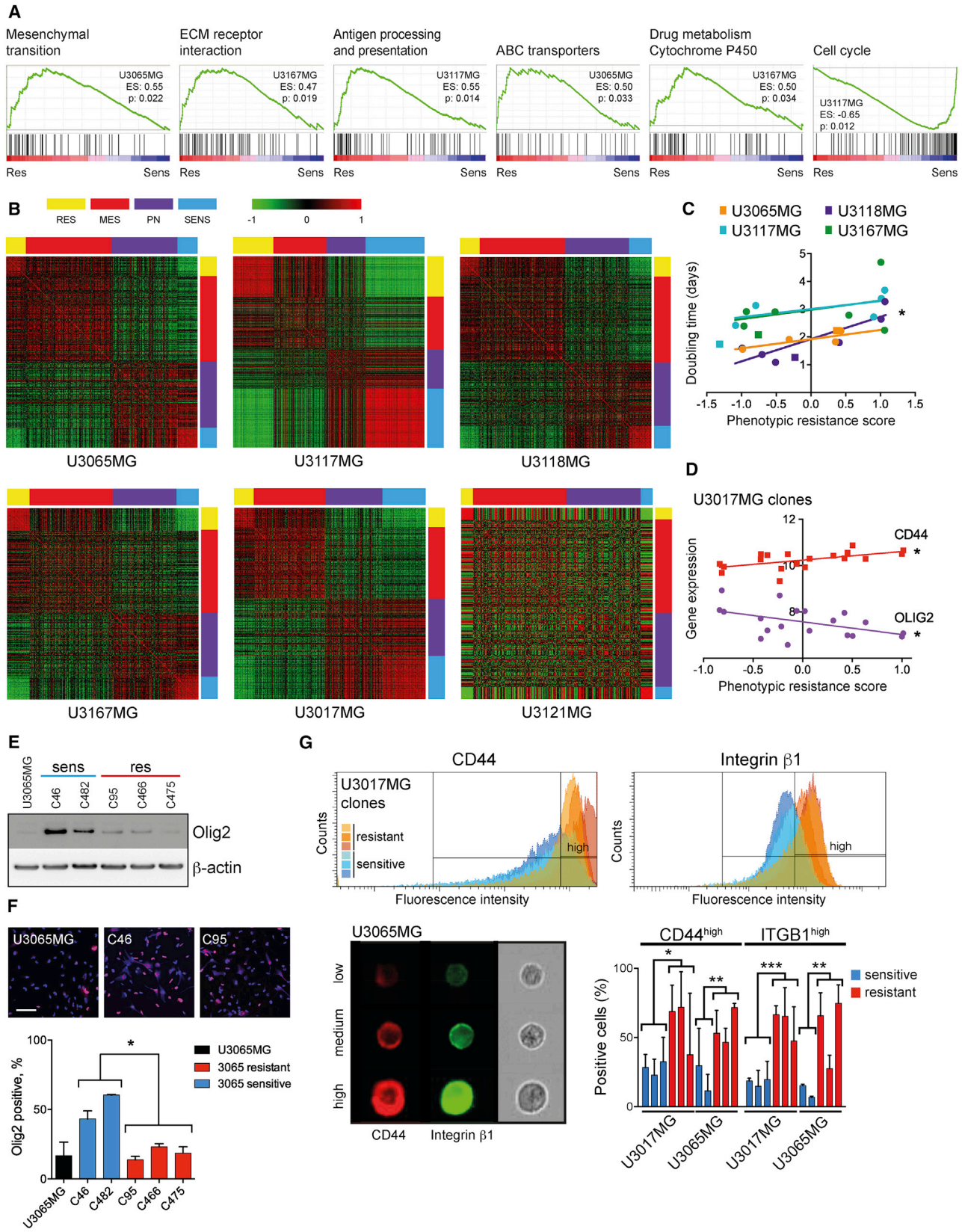

(legend on next page)

gradients, similar to those seen with our GIC clone data (Figures 5F and 5G). Furthermore, in a GIC line dataset characterized by differences in radiosensitivity (Bhat et al., 2013), the metascore of our resistance signature was significantly higher ($p = 0.0034$, unpaired t test) in the resistant group (Figure 5H). The relationship of our signature to the PN-MES axis was further shown in analysis of TCGA samples; on average, MES subtype samples had the highest and PN samples had the lowest resistance signature metascores (Figure 5I). The TCGA samples with the glioma-CpG island methylator phenotype (GCIMP), which typically has a strong PN character, were treated separately and had an even lower resistance signature metascore (Figure 5I). Patients with GCIMP GBM have better prognosis than patients with non-GCIMP tumors (Noushmehr et al., 2010). In TCGA, non-GCIMP tumors are poorly separated in terms of patient survival, regardless of the expression of subtype classifier genes (e.g., PN and MES), which may reflect the intratumoral mosaicism of expression patterns (Patel et al., 2014; Sottoriva et al., 2013). Likewise, our resistance signature (which was related to a MES profile) is not a strong overall predictor of survival in TCGA, but our data indicate that a high resistance metascore was linked to worse prognosis in the extreme cases. When comparing the 20 patients with the highest resistance signature metascore against the 20 patients with the lowest metascore in the non-GCIMP group of tumors, a difference in survival ($p = 0.035$, log rank test) was revealed (Figure S5C), which is in line with the previous finding that patients with high relative strength of the PN signal have better outcome (Patel et al., 2014).

Collectively, our findings indicate that a signature for multitherapy resistance, derived from in vitro cultured GIC clones expanded in isolation, reflects the biology of GBM tumors.

Some Resistant Clones Share CNV Profiles, but Genetic Heterogeneity Does Not Fully Explain the Phenotypic Gradients

Genetic heterogeneity can contribute to cancer drug resistance (Nathanson et al., 2014). Thus, we examined how genetic heterogeneity was related to resistance in our model system. Genome-wide CNV and mutational profiles of the exons of 409 cancer-associated genes were determined in selected clones. Overall, the clones had genetic profiles that were similar to the parental cultures, demonstrating their tumor cell origin. Mutational analysis of seven U3118MG clones representing both resistant and sensitive phenotypes identified only two clone-specific single nucleotide variations (SNVs), both being synonymous substitutions (C736 chr6:152623088G→ C, *SYNE1*, and C150 chr7:100421523G→ A, *EPHB4*). By contrast, clonal variations in the CNV profiles were common. Most of the 28 analyzed clones carried abnormalities that were unique or found only in a subset of the clones, hereafter referred to as clonal CNVs (Figures 6A and S6). The clonal CNVs were mostly broad and in several cases involved whole chromosomes.

To evaluate whether there was a connection between genetic profile and resistance level, we specifically looked at the clonal CNVs shared by a subset of the clones, referred to as sister clones. Sister clones were most common in the U3118MG library, allowing us to construct a dendrogram (Figure 6B). We further displayed the CNV profiles in a heatmap, with clones ordered by their resistance level (Figure 6C). It was evident that sister clones often had a similar resistance level. For instance, the U3118MG sister clones C219, C150, and C688 were all resistant and shared a loss in chr19. The U3167MG sister clones C670 and C723 were both resistant and unified by lack of a broad aberration in chr1. Two sister clones, U3118MG-C38 and U3118MG-C92, were both sensitive and shared a gain in chr3. However, there were also examples of sister clones that had clearly different resistance levels, e.g., U3118MG-C906 (resistant) and U3118MG-C200 (sensitive). In all cases, the sister clones were united by CNVs that involved numerous genes (Table S6). We could not find an obvious driver of MES or PN character in these regions, but the secondary effects of changing the copy number of so many genes are difficult to predict and may influence the cell state.

Three variants of gain involving the PN-associated *SOX2* gene (Verhaak et al., 2010) were seen (Figure 6B), the smallest covering only this gene. This suggested that *SOX2* gain has conferred selective advantage in the U3118MG tumor. The three most resistant U3118MG sister clones lacked *SOX2* gain, which could have displaced them in the MES direction compared to the other clones (Figure 6B). One resistant clone, U3118MG-C508, had chr7q gain (Figures 6A and 6B), where *MET* is located, which could contribute to its MES character (Phillips et al., 2006).

Figure 4. The Multitherapy-Resistant Phenotype Is Associated with a Mesenchymal Profile

(A) Gene set enrichment analysis (GSEA) for Kyoto Encyclopedia of Genes and Genomes (KEGG) categories and a mesenchymal transition signature (Anastassiou et al., 2011). Genes are ordered by correlation to the average drug response. See Table S4 for a detailed GSEA of each library.

(B) Gene similarity matrix comparing the gene sets associated with resistance (RES) and sensitivity (SENS) to MES and PN subtyping genes in all clone libraries. RES and SENS genes were genes with the largest correlation to phenotypic resistance scores. Cutoff r values: ±0.6 U3065MG, U3117MG, and U3017MG; ±0.55 U3118MG; and ±0.67 U3167MG.

(C) Relationship between phenotypic resistance score and proliferation rate for selected clones from four libraries. *$p < 0.05$ (Pearson correlation). Square, parental; circle, clone.

(D) Pearson correlation between OLIG2 and CD44 gene expression and resistance score in the U3017MG clone library. *$p < 0.05$.

(E) Olig2 western blot data on selected sensitive and resistant clones from the U3065MG library. β-actin was used as loading control.

(F) Immunofluorescent staining of Olig2 in selected sensitive and resistant clones (U3065MG library). Upper panel: examples of photographs (Olig2, red; DAPI, blue). Scale bar, 100 μm. Lower panel: quantification of the Olig2 staining, presented as the mean ± SD. See Figures S4C and S4D for Olig2 data on U3017MG clones and U3167MG clones. *$p < 0.05$.

(G) Flow cytometry analysis of CD44 and integrin β1 expression in selected sensitive and resistant clones. Upper panel : overlaid histogram data on U3017MG clones show gating on CD44 and integrin β1 high populations. Bottom left: photographs from the imaging flow cytometry analysis on U3065MG showing representative cells from low-, medium-, and high-intensity gates. Bottom right: quantification of the CD44 and integrin β1 high populations on U3017MG and U3065MG clones, shown as the mean ± SD. *$p < 0.05$; **$p < 0.01$; ***$p < 0.001$ (unpaired t test). See Figure S4E for CD44 and integrin β1 data on U3167MG clones. See also Figure S4 and Tables S4 and S5.

A

DKK3	TMBIM1	FAP	TPCN1	EDIL3
SLC25A43	IGDCC4	SLC9A9	AHNAK	QSOX1
FSTL1	LAMA5	FN1	PLBD2	RBMS3
TBX15	ABCC3	MRO	STOM	LOXL1
TRIM16	DAB2	SLC2A10	RNLS	C1S
ZHX3	CSF1	MVP	SMPD1	SHC1
BLVRB	SLC46A3	HTATIP2	EMILIN1	SERPINB1
PDCD1LG2	OSMR	CYP27A1	OSTF1	FUCA1
CLMP	STAMBPL1	SCPEP1	PER1	MSRB3
NWD1	COPZ2	PPIC	EPHX1	MT1G

B

extracellular space (GO:0005615)
extracellular exosome (GO:0070062)
extracellular membrane-bounded organelle (GO:0065010)
extracellular organelle (GO:0043230)
extracellular vesicle (GO:1903561)
extracellular region part (GO:0044421)
membrane-bounded vesicle (GO:0031988)
vesicle (GO:0031982)
extracellular region (GO:0005576)

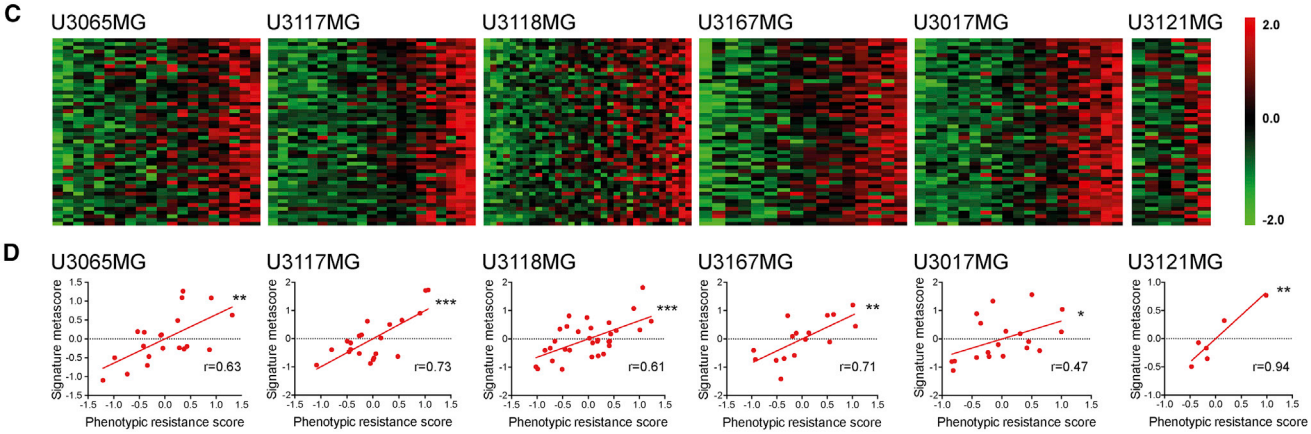

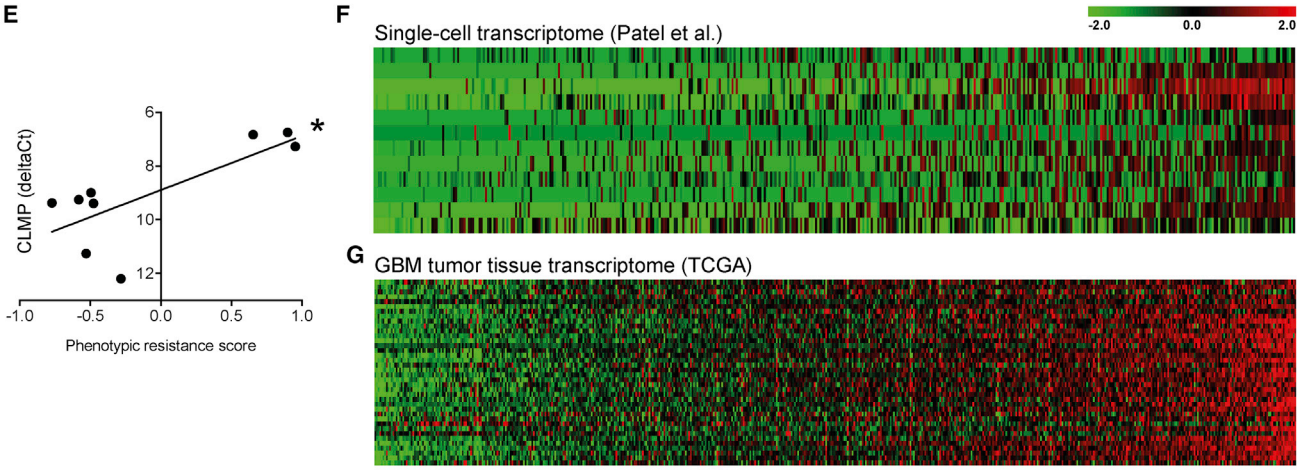

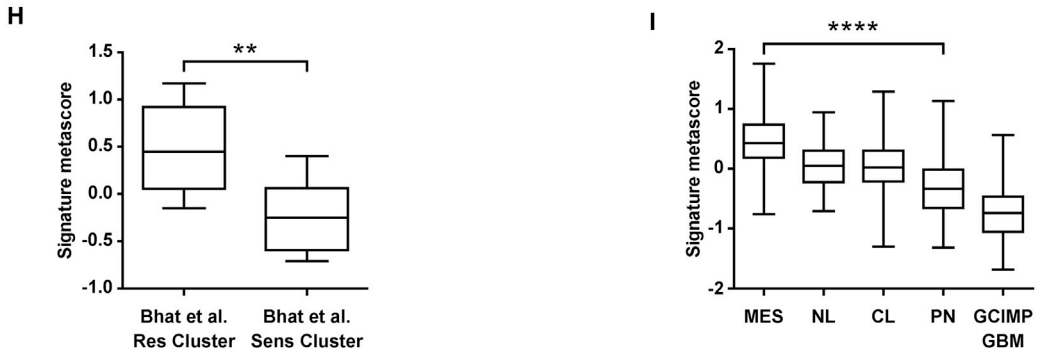

(legend on next page)

In summary, we observed clonal genetic heterogeneity, primarily manifested on the CNV level but with no common denominator for resistance extending across libraries. The continuous phenotypic gradients found among clones could not readily be explained by their genetics, but the similar resistance level frequently seen in sister clones suggests that broad CNVs may influence positioning in the sensitivity-resistance gradient. Alternatively, they have inherited their phenotypes from a recent common ancestor by a non-genetic mechanism.

The Multitherapy-Resistant and Multitherapy-Sensitive GIC States Display Methylation Pattern Differences that Include MES Master Regulator Promoter Regions

Epigenetic mechanisms can govern stable, but reversible, cellular transitions related to altered function, e.g., epithelial-to-mesenchymal transition (EMT) (Thiery et al., 2009). The semi-stability of our phenotypes is thus suggestive of epigenetic regulation. Alteration in DNA methylation is of clinical importance in GBM (Hegi et al., 2005; Noushmehr et al., 2010). We therefore analyzed the global DNA methylation pattern of 16 representative clones from the U3065MG library. Previously defined differentially methylated regions (DMRs), including DMRs associated with cancer (CDMR) and reprogramming (RDMR), were overrepresented among the most variable methylation sites (Figure 7A). When comparing the methylation data with the resistance signature metascores, the frequency histogram of correlation coefficients displayed a trimodal distribution and had clearly longer tails than those of the distribution obtained with permutated metascores (Figure 7B). Thus, a subset of the methylation sites altered their methylation level, either upward or downward, in conjunction with increased resistance. These resistance-associated methylation sites were strongly enriched in "enhancer" annotations, especially those with decreased methylation (Figure 7C). This indicates that a large part of the DNA methylation effects is connected to enhancer-mediated regulation of gene expression.

We next extracted methylation signatures that were positively (repression signature) and negatively (activation signature) linked to resistance (Figure 7D). The signatures were filtered to include only methylation sites, where changed methylation status affected gene expression. The activation signature contained promoter-associated methylation sites of *FOSL2* and *RUNX1*, which have been pointed out as master regulators of the MES GBM subtype (Carro et al., 2010). In addition, a third putative MES master regulator, *BHLHE40*, was found just below the threshold used for selecting the activation signature (data not shown). Overall, the strongest link to resistance across libraries was seen for *FOSL2*, whose expression levels significantly correlated with the resistance signature metascore in five of six libraries (Figure S7). The *FOSL2* methylation site was found in a CpG island shelf region, which has been previously identified as an RDMR (Figure 7E) (Doi et al., 2009). When we compared the average methylation level of this RDMR region in the TCGA dataset, we found that the MES GBM subtype samples had a lower methylation level than that of PN samples ($p = 0.007$, unpaired t test) (Figure 7F). Furthermore, the GCIMP samples were highly methylated in these regions, in line with having the lowest resistance signature metascore (Figure 5I).

Altogether, the results support the assumption that the resistance phenotype of our GIC clones is associated with an epigenetically stabilized mesenchymal cell state. More specifically, we detect changes in the DNA methylation pattern of regulatory elements, including master regulators of the MES subtype in glioblastoma.

DISCUSSION

Using a large-scale clonal analysis of GICs, we have discovered a multitherapy sensitivity-resistance gradient coupled to a corresponding continuous PN-MES axis, which constitutes a distinct form of heterogeneity in the GIC compartment. Our results fit with a model in which an epigenetic drift between PN- and MES-like cell states operates in parallel with genetic diversification and selection to generate a heterogeneous tumor cell population. This GIC heterogeneity appeared to be widespread, as it was found in all analyzed tumor samples, each representing only a minor fraction of the tumor mass.

The present study goes beyond previous functional studies on GIC clones (Meyer et al., 2015; Piccirillo et al., 2015) in that it identifies a continuum of responses to radiation and multiple drugs. The finding that resistant clones displayed a uniformly poor response to multiple treatments points toward a general, not target-specific, resistance mechanism; hence, we use the term multitherapy resistance. Resistance was clearly associated with a MES-like cell state of the GIC clones, which is consistent with previous observations on mass cultures of GBM (Bhat et al., 2013; Mao et al., 2013). In addition, in carcinoma, a mesenchymal phenotype is associated with increased resistance (Thiery et al., 2009).

Figure 5. A Gene Expression Signature for the Multitherapy-Resistant GIC State Identifies Gradients in Both Single-Cell and Tumor Sample Datasets

(A) A 50 gene transcriptome resistance signature optimized for best performance across all libraries.
(B) Representative Gene Ontology (GO) terms enriched in the resistance signature.
(C) Heatmaps of the resistance signature expression values (*Z* scores, rows) in all six GIC libraries. Clones (columns) are ordered by their signature metascore.
(D) Pearson correlation between the resistance signature metascore and the phenotypic resistance score. *$p < 0.05$; **$p < 0.01$; ***$p < 0.001$.
(E) Pearson correlation between qPCR data for the resistance signature gene CLMP and average drug response for ten previously uncharacterized clones from the U3065MG library. *$p < 0.05$.
(F) Heatmap of our resistance signature in a GBM single-cell transcriptome dataset (Patel et al., 2014).
(G) Heatmap of our resistance signature in TCGA GBM tumor transcriptome data (http://tcga-data.nci.nih.gov).
(H) Comparison of the metascores for our resistance signature in the radioresistant and radiosensitive GIC clusters defined in Bhat et al. (2013). **$p < 0.01$ (unpaired t test).
(I) Resistance signature metascore in the TCGA GBM molecular subtypes dataset. ****$p < 0.0001$ (one-way ANOVA with Tukey's post hoc test).
See also Figures S5A and S5B.

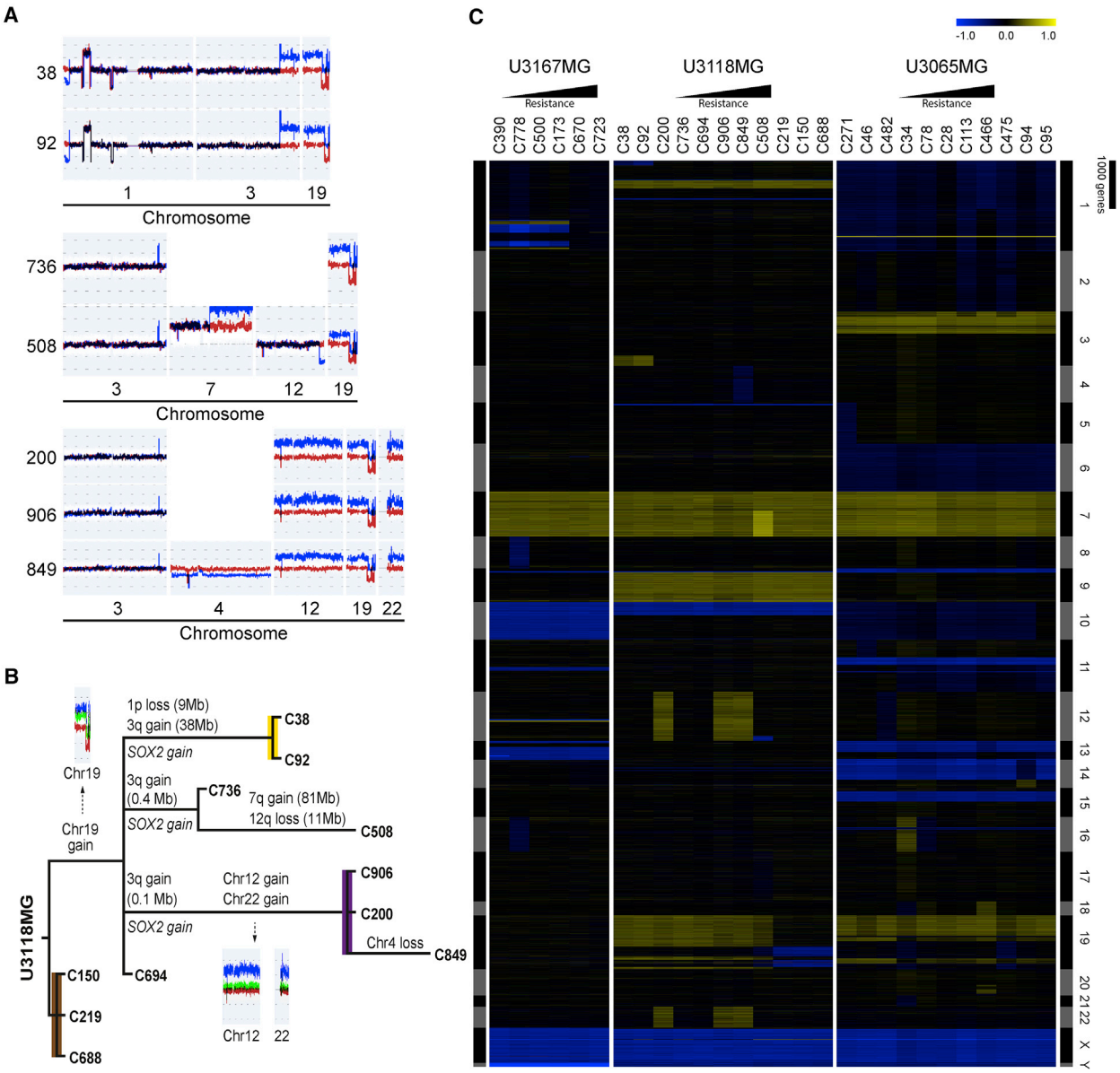

Figure 6. Some Resistant Clones Share CNV Profiles, but Genetic Heterogeneity Does Not Fully Explain the Phenotypic Gradients

(A) Clone-specific CNVs (blue) in the U3118MG library overlaid with a clone without that aberration (red). See Figure S6 for data on clones from four libraries.

(B) Dendrogram showing genetic lineages based on clone-specific CNV alterations in the U3118MG clonal library. Inserts show the parental line (green) overlaid with clones with (blue) and without (red) specific aberrations. Colored clades (yellow, purple, and brown) are also indicated in the treatment response heatmap in Figure 2E.

(C) Heatmaps of CNV values (average log2 ratios) for all genes in clones from three libraries. Clones are ordered by resistance level, and genes are ordered by chromosomal position.

See also Figure S6 and Table S6.

The continuous phenotypic gradients contradict a major role of genetic aberrations as drivers of resistance. Furthermore, we did not find clone-specific genetic variations in known MES drivers or regulators, such as *NF1*, *FOSL2*, *STAT3*, *RUNX1* and *BHLHE40* (Carro et al., 2010; Ozawa et al., 2014), with exception of *MET* gain in one resistant clone. Nevertheless, the influence of broad CNVs on the transcriptome is difficult to assess and could alter therapy response. Several sister clones had similar resistance levels, which could be a result of such genetic influences. An alternative explanation would be that sister clones have inherited the same epigenetic profile (Mazor et al., 2015).

Whereas phenotypic plasticity is likely to underlie the sensitivity-resistance gradients, clones can be expanded with retained phenotypic profiles, which is strong evidence for stability.

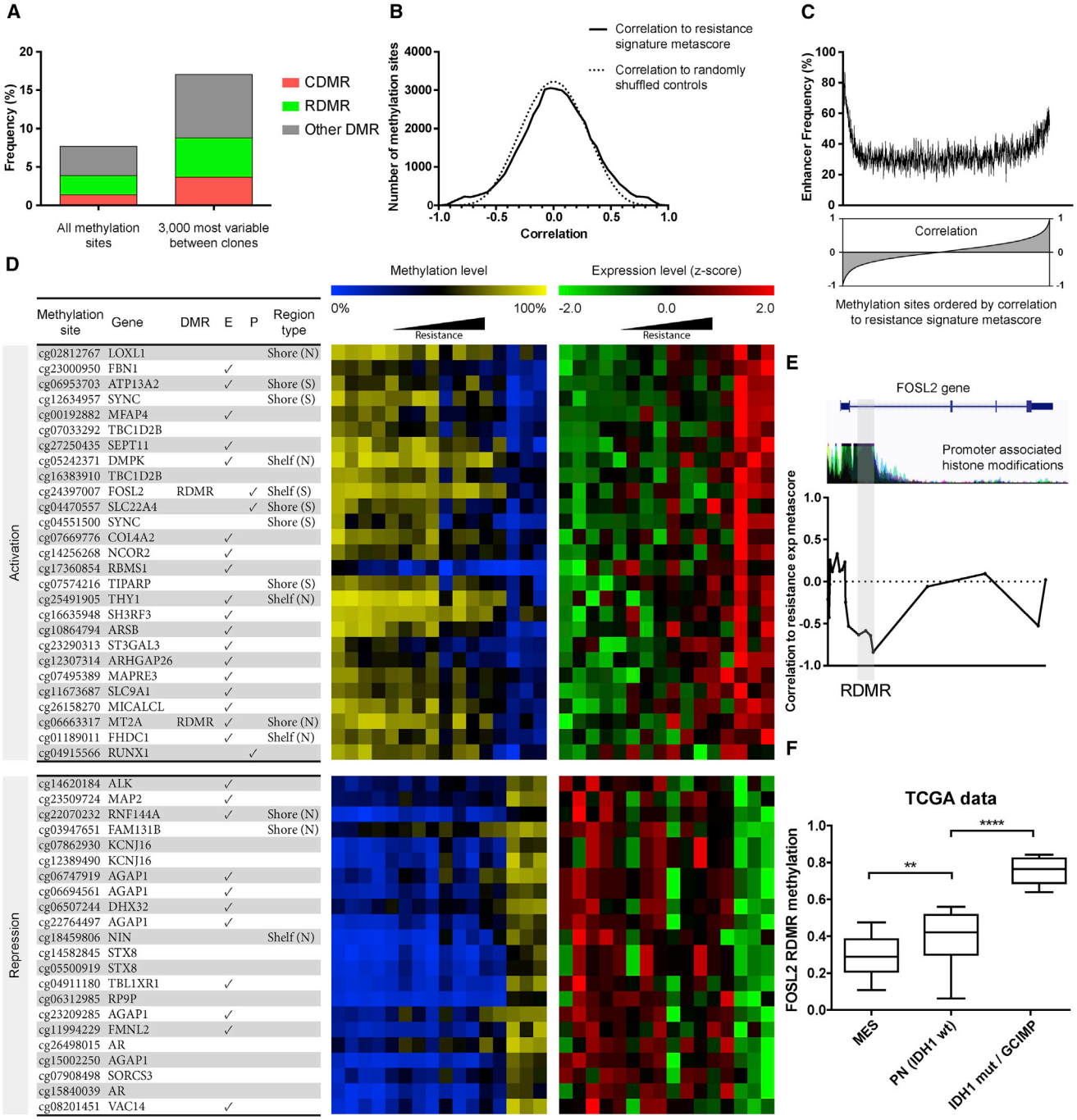

Methylation site	Gene	DMR	E	P	Region type
cg02812767	LOXL1				Shore (N)
cg23000950	FBN1		✓		
cg06953703	ATP13A2		✓		Shore (S)
cg12634957	SYNC				Shore (S)
cg00192882	MFAP4		✓		
cg07033292	TBC1D2B				
cg27250435	SEPT11		✓		
cg05242371	DMPK		✓		Shelf (N)
cg16383910	TBC1D2B				
cg24397007	FOSL2	RDMR		✓	Shelf (S)
cg04470557	SLC22A4			✓	Shore (S)
cg04551500	SYNC				Shore (S)
cg07669776	COL4A2		✓		
cg14256268	NCOR2		✓		
cg17360854	RBMS1		✓		
cg07574216	TIPARP				Shore (S)
cg25491905	THY1		✓		Shelf (N)
cg16635948	SH3RF3		✓		
cg10864794	ARSB		✓		
cg23290313	ST3GAL3		✓		
cg12307314	ARHGAP26		✓		
cg07495389	MAPRE3		✓		
cg11673687	SLC9A1		✓		
cg26158270	MICALCL		✓		
cg06663317	MT2A	RDMR	✓		Shore (N)
cg01189011	FHDC1		✓		Shelf (N)
cg04915566	RUNX1			✓	
cg14620184	ALK		✓		
cg23509724	MAP2		✓		
cg22070232	RNF144A		✓		Shore (N)
cg03947651	FAM131B				Shore (N)
cg07862930	KCNJ16				
cg12389490	KCNJ16				
cg06747919	AGAP1		✓		
cg06694561	AGAP1		✓		
cg06507244	DHX32		✓		
cg22764497	AGAP1		✓		
cg18459806	NIN				Shelf (N)
cg14582845	STX8				
cg05500919	STX8				
cg04911180	TBL1XR1		✓		
cg06312985	RP9P				
cg23209285	AGAP1		✓		
cg11994229	FMNL2		✓		
cg26498015	AR				
cg15002250	AGAP1				
cg07908498	SORCS3				
cg15840039	AR				
cg08201451	VAC14		✓		

Figure 7. The Multiresistant and Sensitive GIC States Display Methylation Pattern Differences that Include MES Master Regulator Promoter Regions

(A) Frequencies of differentially methylated regions (DMRs), including cancer DMR and reprogramming DMR (CDMR and RDMR, respectively), in the most variable methylation sites among clones of the U3065MG library.

(B) Distribution of correlation coefficients comparing the most variable methylation sites with the resistance signature metascore in the U3065MG library. The dotted line represents mean distribution of random shuffled metascores.

(C) Enrichment analysis of enhancer region frequencies in resistance-associated differentially methylated sites of the U3065MG library.

(D) Activation and repression methylation signatures (negatively < −0.8 correlated and positively > 0.8 correlated, respectively) linked to resistance. The activation signature included master regulators of the MES GBM subtype, *FOSL2* and *RUNX1*.

(legend continued on next page)

There were examples of clones changing phenotype, but evidently transition between the GIC states must be slow.

This is suggestive of epigenetic regulation, and we found an altered DNA methylation pattern in resistant clones, which included MES master regulators (Carro et al., 2010). For one of them, *FOSL2*, we could differentiate the MES and PN subtypes in TCGA data using only a few promoter-associated methylation sites. This *FOSL2* region has been identified as a reprogramming-associated DMR in relation to induced pluripotency of fibroblasts (Doi et al., 2009). It is tempting to speculate that DNA hypermethylation-mediated inactivation of MES master regulators, such as *FOSL2*, contributes to the strong PN character of GCIMP tumors (Noushmehr et al., 2010). Our methylation signature was also strongly enriched in methylation sites coupled to enhancer regions. This is intriguing, because methylation dynamics of enhancer regions has been linked to cancer cell plasticity (Bell et al., 2016). Epigenetically mediated drift between PN and MES cell states in the GIC compartment is probably part of the explanation of the subtype mosaicism observed in tumor tissues (Patel et al., 2014; Sottoriva et al., 2013). This view is supported by the identification of "hybrid" cell states with mixed subtype characteristics in single-cell analysis of GBM (Patel et al., 2014).

It is tempting to compare our findings with the dynamic and reversible EMT process (Thiery et al., 2009), which also is believed to be epigenetically regulated (Tam and Weinberg, 2013). In GBM, the term proneural-to-mesenchymal transition (PMT) is increasingly being used (Lau et al., 2015; Mao et al., 2013; Piao et al., 2013). Both EMT and PMT are induced by extrinsic factors, e.g., transforming growth factor β (TGF-β) in carcinomas (Thiery et al., 2009) and tumor necrosis factor alpha (TNF-α) and nuclear factor κB (NF-κB) activation (Bhat et al., 2013) or radiation exposure in GBM (Halliday et al., 2014). Our cultures were derived from single GICs expanded in isolation, thus ruling out any direct influence from paracrine mediators from other cell types. However, it is likely that the phenotypic profiles were molded in vivo, e.g., by the exposure to cytokines and other extrinsic cues generated by inflammatory cells, vasculature, hypoxia, etc. This view has wide implications, because it infers that our highly reductionistic model system, i.e., clonal tumor cell populations expanded in vitro, carries a memory imprinted by the complex tumor microenvironment.

Most tumors appear to display regional differences in the distribution of PN and MES cells, which confounds molecular classification of GBM based on single biopsies and impairs its prognostic value (Patel et al., 2014; Sottoriva et al., 2013). Still, non-GCIMP patients with a "pure" PN subtype signal show a survival benefit compared to those with heterogeneous samples (Patel et al., 2014). In analogy with this, we observed a survival benefit for patients displaying the weakest resistance signature. Altogether, the MES and PN signatures have limited value when comparing patient samples but may be useful to identify treatment-resistant cell populations within tumors.

Following the idea that PN-MES-related intratumoral heterogeneity is an important factor in the uniformly poor prognosis of non-GCIMP GBM, targeting this heterogeneity per se may be a way forward to improve treatment. Blockage of signal transducer and activator of transcription 3 (STAT3) activation was shown to inhibit radiation-induced PMT and resulted in prolonged survival of mice with PN GBM in response to radiation therapy (Lau et al., 2015). Our normal distributed data suggest that a spontaneous mesenchymal-to-proneural transition (MPT) also exists, counteracting PMT. Elucidating the underlying pathways of MPT may identify new strategies to sensitize resistant tumor cells to cytotoxic agents.

In summary, we hypothesize a model in which functional GIC heterogeneity is formed by an epigenetically regulated drift between a more resistant MES cell state and a more sensitive PN state. Our clonal analyses reveal a distinct form of heterogeneity that can direct the development of new treatment strategies for GBM.

EXPERIMENTAL PROCEDURES

See also Supplemental Experimental Procedures.

Cell Culture and Cloning Procedure

Fresh tumor samples were obtained from adult patients with GBM at the Uppsala University Hospital after patient consent and approval by the regional ethical review board. Tumor surgical samples were dissociated and pre-conditioned by brief culturing in neural stem cell (NSC) media (Neurobasal+DMEM/F12 media supplemented with N2, B27, epidermal growth factor [EGF], and basic fibroblast growth factor [bFGF]). Clones were primarily generated by single-cell fluorescence-activated cell sorting (FACS) of pre-conditioned tumor cells into laminin-coated 384-well plates, followed by sequential passaging of subconfluent cultures up to 35-mm Primaria tissue culture dishes. Fifty-three clones representing all libraries and phenotypes were analyzed using short tandem repeat (STR) profiling and showed no sign of contaminations (Table S7).

Radiation and Drug Response Experiments

Cells were seeded in laminin-coated 384-well plates (1,000 cells/well) 24 hr before treatment. Cells were exposed to 4 Gy γ-radiation using a 137Cs source (Gammacell 40 Exactor, Best Theratronics). Control cultures were left unexposed. TMZ (125 μM) was added 2 hr before γ-radiation, when it was combined. Cell survival was measured 6 days later using the fluorometric microculture cytotoxicity assay (FMCA) protocol (Supplemental Experimental Procedures).

Drugs were dissolved in DMSO and cell survival was measured 72 hr after drug exposure, using the FMCA protocol.

Molecular Profiling

Transcriptome, CNV, and STR analyses were performed according to standard protocols for Human Transcriptome Array 2.0, Affymetrix Cytoscan HD arrays (Affymetrix), and the AB ampFISTR Identifier Amplification Kit (Applied Biosystems, Thermo Fisher Scientific). Exon sequencing of 409 cancer-associated genes was made with Ion AmpliSeq Comprehensive Cancer Panel

(E) Negative Pearson correlation between resistance signature metascore and methylation sites in the promoter-associated CpG island shore and shelf region of *FOSL2*, designated as an RDMR (gray area). The *FOSL2* exons and promoter regions (University of California Santa Cruz [UCSC] genome browser hg19) are indicated.

(F) Methylation level of the *FOSL2* RDMR in the TCGA GBM dataset. $^{**}p < 0.01$; $^{****}p < 0.0001$ (unpaired t test).

See also Figure S7.

(Ion Torrent, Life Technologies). DNA methylation was analyzed using the HumanMethylation450 BeadChip array (Illumina). Expression, CNV, and methylation data are available via GEO: GSE89401, GSE89398, GSE89399, and GSE89400. Transcriptome data were normalized in the Affymetrix Expression console using robust multiarray average (RMA).

Xenograft Experiments

Animal experiments were performed in accordance with the regulations at Upsala University after approval by the local animal ethics committee. Neonatal NOD-SCID mice were injected intracerebrally with 1×10^5 cells. Animals were monitored and euthanized upon signs of illness and analyzed for xenograft tumors.

Statistical Analyses

Calculations were made in GraphPad Prism (GraphPad), R (The R Project) and Excel (Microsoft). Clustering, heatmaps, and PCA were made in MultiExperiment Viewer (MeV, TM4). TCGA data were downloaded from TCGA data portal. Gene ontology analysis was made at http://geneontology.org/.

The phenotypic resistance score was the mean of the *Z* score values for AUCs (drugs) and survival indexes (SIs) (radiation) in each clone library. Library-specific resistance- and sensitivity-associated genes were the largest positively and negatively correlating (Pearson) transcripts when compared to the phenotypic resistance scores. The 5,000 most variable genes were used, and cutoffs were set based on permutation analysis (Supplemental Experimental Procedures).

The resistance signature was made by combining all library-specific resistance-associated genes and selecting the 50 with the largest average correlation to the phenotypic resistance score across all libraries. The signature metascore was calculated as the mean value of all signature gene expression values. The methylation signature was made by analysis of the correlations between the 10% most variable methylation sites and the resistance signature metascores. Cutoffs were set based on permutation analysis (Supplemental Experimental Procedures).

ACCESSION NUMBERS

The accession numbers for the expression, CNV, and methylation data reported in this paper are GEO: GSE89401, GSE89398, GSE89399, and GSE89400.

SUPPLEMENTAL INFORMATION

Supplemental Information includes Supplemental Experimental Procedures, seven figures, and seven tables and can be found with this article online at http://dx.doi.org/10.1016/j.celrep.2016.11.056.

AUTHOR CONTRIBUTIONS

A.S., B.S., and B.W. conceived and designed the study; A.S. and M.N. coordinated the experimental work; A.S., M.N., and A.W. made the clone libraries; A.S., M.N., C.H., T.B., M.J., Y.X., D.S., F.N., A.H., M.K., Z.N-A., M.B., A.W., and M.S. performed the experiments; A.S., M.N., C.H., T.B., M.J., M.G., M.F., and B.S. analyzed the data; G.H. contributed with surgical samples; A.S., B.S., M.N., T.B., and B.W. wrote the manuscript; and C.H., M.J., L.U., M.G., M.F., and R.L. contributed to the final manuscript and/or the interpretations.

ACKNOWLEDGMENTS

This study was supported by grants from the Knut and Alice Wallenberg Foundation (2013.0280). We thank the SciLifeLab core facilities: the Uppsala BioVis facility, the Uppsala Tissue Profiling Facility, the Uppsala Array Platform, and the National Genomic Infrastructure. We also thank Erika Dalmo for help with qPCR and Dr. Irina Alafuzoff for support in malignancy grade determination of xenograft tumors. B.W. and A.S. were supported by grants from the Swedish Cancer Society (150670) and A.S. was supported by a grant from the Uppsala University Hospital.

Received: May 26, 2015
Revised: June 23, 2016
Accepted: November 17, 2016
Published: December 13, 2016

REFERENCES

Anastassiou, D., Rumjantseva, V., Cheng, W., Huang, J., Canoll, P.D., Yamashiro, D.J., and Kandel, J.J. (2011). Human cancer cells express Slug-based epithelial-mesenchymal transition gene expression signature obtained in vivo. BMC Cancer *11*, 529.

Bao, S., Wu, Q., McLendon, R.E., Hao, Y., Shi, Q., Hjelmeland, A.B., Dewhirst, M.W., Bigner, D.D., and Rich, J.N. (2006). Glioma stem cells promote radioresistance by preferential activation of the DNA damage response. Nature *444*, 756–760.

Beier, D., Hau, P., Proescholdt, M., Lohmeier, A., Wischhusen, J., Oefner, P.J., Aigner, L., Brawanski, A., Bogdahn, U., and Beier, C.P. (2007). CD133(+) and CD133(−) glioblastoma-derived cancer stem cells show differential growth characteristics and molecular profiles. Cancer Res. *67*, 4010–4015.

Bell, R.E., Golan, T., Sheinboim, D., Malcov, H., Amar, D., Salamon, A., Liron, T., Gelfman, S., Gabet, Y., Shamir, R., and Levy, C. (2016). Enhancer methylation dynamics contribute to cancer plasticity and patient mortality. Genome Res. *26*, 601–611.

Bhat, K.P.L., Balasubramaniyan, V., Vaillant, B., Ezhilarasan, R., Hummelink, K., Hollingsworth, F., Wani, K., Heathcock, L., James, J.D., Goodman, L.D., et al. (2013). Mesenchymal differentiation mediated by NF-κB promotes radiation resistance in glioblastoma. Cancer Cell *24*, 331–346.

Bleau, A.M., Hambardzumyan, D., Ozawa, T., Fomchenko, E.I., Huse, J.T., Brennan, C.W., and Holland, E.C. (2009). PTEN/PI3K/Akt pathway regulates the side population phenotype and ABCG2 activity in glioma tumor stem-like cells. Cell Stem Cell *4*, 226–235.

Bonnet, D., and Dick, J.E. (1997). Human acute myeloid leukemia is organized as a hierarchy that originates from a primitive hematopoietic cell. Nat. Med. *3*, 730–737.

Carro, M.S., Lim, W.K., Alvarez, M.J., Bollo, R.J., Zhao, X., Snyder, E.Y., Sulman, E.P., Anne, S.L., Doetsch, F., Colman, H., et al. (2010). The transcriptional network for mesenchymal transformation of brain tumours. Nature *463*, 318–325.

Doi, A., Park, I.H., Wen, B., Murakami, P., Aryee, M.J., Irizarry, R., Herb, B., Ladd-Acosta, C., Rho, J., Loewer, S., et al. (2009). Differential methylation of tissue- and cancer-specific CpG island shores distinguishes human induced pluripotent stem cells, embryonic stem cells and fibroblasts. Nat. Genet. *41*, 1350–1353.

Halliday, J., Helmy, K., Pattwell, S.S., Pitter, K.L., LaPlant, Q., Ozawa, T., and Holland, E.C. (2014). In vivo radiation response of proneural glioma characterized by protective p53 transcriptional program and proneural-mesenchymal shift. Proc. Natl. Acad. Sci. USA *111*, 5248–5253.

Hegi, M.E., Diserens, A.C., Gorlia, T., Hamou, M.F., de Tribolet, N., Weller, M., Kros, J.M., Hainfellner, J.A., Mason, W., Mariani, L., et al. (2005). MGMT gene silencing and benefit from temozolomide in glioblastoma. N. Engl. J. Med. *352*, 997–1003.

Lathia, J.D., Mack, S.C., Mulkearns-Hubert, E.E., Valentim, C.L., and Rich, J.N. (2015). Cancer stem cells in glioblastoma. Genes Dev. *29*, 1203–1217.

Lau, J., Ilkhanizadeh, S., Wang, S., Miroshnikova, Y.A., Salvatierra, N.A., Wong, R.A., Schmidt, C., Weaver, V.M., Weiss, W.A., and Persson, A.I. (2015). STAT3 blockade inhibits radiation-induced malignant progression in glioma. Cancer Res. *75*, 4302–4311.

Lee, J., Kotliarova, S., Kotliarov, Y., Li, A., Su, Q., Donin, N.M., Pastorino, S., Purow, B.W., Christopher, N., Zhang, W., et al. (2006). Tumor stem cells derived from glioblastomas cultured in bFGF and EGF more closely mirror the phenotype and genotype of primary tumors than do serum-cultured cell lines. Cancer Cell *9*, 391–403.

Ligon, K.L., Huillard, E., Mehta, S., Kesari, S., Liu, H., Alberta, J.A., Bachoo, R.M., Kane, M., Louis, D.N., Depinho, R.A., et al. (2007). Olig2-regulated

lineage-restricted pathway controls replication competence in neural stem cells and malignant glioma. Neuron *53*, 503–517.

Liu, G., Yuan, X., Zeng, Z., Tunici, P., Ng, H., Abdulkadir, I.R., Lu, L., Irvin, D., Black, K.L., and Yu, J.S. (2006). Analysis of gene expression and chemoresistance of CD133+ cancer stem cells in glioblastoma. Mol. Cancer *5*, 67.

Mao, P., Joshi, K., Li, J., Kim, S.-H., Li, P., Santana-Santos, L., Luthra, S., Chandran, U.R., Benos, P.V., Smith, L., et al. (2013). Mesenchymal glioma stem cells are maintained by activated glycolytic metabolism involving aldehyde dehydrogenase 1A3. Proc. Natl. Acad. Sci. USA *110*, 8644–8649.

Mazor, T., Pankov, A., Johnson, B.E., Hong, C., Hamilton, E.G., Bell, R.J., Smirnov, I.V., Reis, G.F., Phillips, J.J., Barnes, M.J., et al. (2015). DNA methylation and somatic mutations converge on the cell cycle and define similar evolutionary histories in brain tumors. Cancer Cell *28*, 307–317.

Meyer, M., Reimand, J., Lan, X., Head, R., Zhu, X., Kushida, M., Bayani, J., Pressey, J.C., Lionel, A.C., Clarke, I.D., et al. (2015). Single cell-derived clonal analysis of human glioblastoma links functional and genomic heterogeneity. Proc. Natl. Acad. Sci. USA *112*, 851–856.

Nathanson, D.A., Gini, B., Mottahedeh, J., Visnyei, K., Koga, T., Gomez, G., Eskin, A., Hwang, K., Wang, J., Masui, K., et al. (2014). Targeted therapy resistance mediated by dynamic regulation of extrachromosomal mutant EGFR DNA. Science *343*, 72–76.

Noushmehr, H., Weisenberger, D.J., Diefes, K., Phillips, H.S., Pujara, K., Berman, B.P., Pan, F., Pelloski, C.E., Sulman, E.P., Bhat, K.P., et al.; Cancer Genome Atlas Research Network (2010). Identification of a CpG island methylator phenotype that defines a distinct subgroup of glioma. Cancer Cell *17*, 510–522.

Ozawa, T., Riester, M., Cheng, Y.-K., Huse, J.T., Squatrito, M., Helmy, K., Charles, N., Michor, F., and Holland, E.C. (2014). Most human non-GCIMP glioblastoma subtypes evolve from a common proneural-like precursor glioma. Cancer Cell *26*, 288–300.

Patel, A.P., Tirosh, I., Trombetta, J.J., Shalek, A.K., Gillespie, S.M., Wakimoto, H., Cahill, D.P., Nahed, B.V., Curry, W.T., Martuza, R.L., et al. (2014). Single-cell RNA-seq highlights intratumoral heterogeneity in primary glioblastoma. Science *344*, 1396–1401.

Phillips, H.S., Kharbanda, S., Chen, R., Forrest, W.F., Soriano, R.H., Wu, T.D., Misra, A., Nigro, J.M., Colman, H., Soroceanu, L., et al. (2006). Molecular subclasses of high-grade glioma predict prognosis, delineate a pattern of disease progression, and resemble stages in neurogenesis. Cancer Cell *9*, 157–173.

Piao, Y., Liang, J., Holmes, L., Henry, V., Sulman, E., and de Groot, J.F. (2013). Acquired resistance to anti-VEGF therapy in glioblastoma is associated with a mesenchymal transition. Clin. Cancer Res. *19*, 4392–4403.

Piccirillo, S.G., Colman, S., Potter, N.E., van Delft, F.W., Lillis, S., Carnicer, M.J., Kearney, L., Watts, C., and Greaves, M. (2015). Genetic and functional diversity of propagating cells in glioblastoma. Stem Cell Reports *4*, 7–15.

Pollard, S.M., Yoshikawa, K., Clarke, I.D., Danovi, D., Stricker, S., Russell, R., Bayani, J., Head, R., Lee, M., Bernstein, M., et al. (2009). Glioma stem cell lines expanded in adherent culture have tumor-specific phenotypes and are suitable for chemical and genetic screens. Cell Stem Cell *4*, 568–580.

Singh, S.K., Clarke, I.D., Terasaki, M., Bonn, V.E., Hawkins, C., Squire, J., and Dirks, P.B. (2003). Identification of a cancer stem cell in human brain tumors. Cancer Res. *63*, 5821–5828.

Sottoriva, A., Spiteri, I., Piccirillo, S.G., Touloumis, A., Collins, V.P., Marioni, J.C., Curtis, C., Watts, C., and Tavaré, S. (2013). Intratumor heterogeneity in human glioblastoma reflects cancer evolutionary dynamics. Proc. Natl. Acad. Sci. USA *110*, 4009–4014.

Stupp, R., Mason, W.P., van den Bent, M.J., Weller, M., Fisher, B., Taphoorn, M.J., Belanger, K., Brandes, A.A., Marosi, C., Bogdahn, U., et al.; European Organisation for Research and Treatment of Cancer Brain Tumor and Radiotherapy Groups; National Cancer Institute of Canada Clinical Trials Group (2005). Radiotherapy plus concomitant and adjuvant temozolomide for glioblastoma. N. Engl. J. Med. *352*, 987–996.

Szerlip, N.J., Pedraza, A., Chakravarty, D., Azim, M., McGuire, J., Fang, Y., Ozawa, T., Holland, E.C., Huse, J.T., Jhanwar, S., et al. (2012). Intratumoral heterogeneity of receptor tyrosine kinases EGFR and PDGFRA amplification in glioblastoma defines subpopulations with distinct growth factor response. Proc. Natl. Acad. Sci. USA *109*, 3041–3046.

Tam, W.L., and Weinberg, R.A. (2013). The epigenetics of epithelial-mesenchymal plasticity in cancer. Nat. Med. *19*, 1438–1449.

Thiery, J.P., Acloque, H., Huang, R.Y., and Nieto, M.A. (2009). Epithelial-mesenchymal transitions in development and disease. Cell *139*, 871–890.

Verhaak, R.G., Hoadley, K.A., Purdom, E., Wang, V., Qi, Y., Wilkerson, M.D., Miller, C.R., Ding, L., Golub, T., Mesirov, J.P., et al.; Cancer Genome Atlas Research Network (2010). Integrated genomic analysis identifies clinically relevant subtypes of glioblastoma characterized by abnormalities in PDGFRA, IDH1, EGFR, and NF1. Cancer Cell *17*, 98–110.

Visvader, J.E., and Lindeman, G.J. (2008). Cancer stem cells in solid tumours: accumulating evidence and unresolved questions. Nat. Rev. Cancer *8*, 755–768.

Xie, Y., Bergström, T., Jiang, Y., Johansson, P., Marinescu, V.D., Lindberg, N., Segerman, A., Wicher, G., Niklasson, M., Baskaran, S., et al. (2015). The human glioblastoma cell culture resource: validated cell models representing all molecular subtypes. EBioMedicine *2*, 1351–1363.